Gate-Voltage Control of Quantum Yield in Monolayer Transition-Metal Dichalcogenide

Maksym V. Strikha[1,2] Anatolii I. Kurchak[2] and Anna N. Morozovska[3,*]

[1] *Taras Shevchenko Kyiv National University, Faculty of RECS, Kyiv, Ukraine*

[2] *V. Lashkariov Institute of Semiconductor Physics of the National Academy of Sciences of Ukraine, Kyiv, Ukraine*

[3] *Institute of Physics of the National Academy of Sciences of Ukraine, Kyiv, Ukraine*

(Received 23 September 2019; revised manuscript received 10 November 2019; published 23 January 2020)

Two-dimensional (2D) transition-metal dichalcogenide (TMD) monolayers, which reveal remarkable semiconductor properties, are the subject of active experimental research. It should be noted that, unlike bulk TMDs, which are indirect-band semiconductors, 2D TMD monolayers have the extreme points of the conduction and valence bands at the same K and K' points of the Brillouin zone. Therefore, they are direct-band semiconductors and can claim to be widely used in optoelectronics devices. Recently, it has been shown experimentally that quantum yield in MoS_2 and WSe_2 monoatomic layers can reach values close to unity when electrostatic doping makes them intrinsic semiconductors. However, the available theoretical description does not provide an understanding of the physical mechanisms underlying the gate voltage control of quantum yield. This work is an attempt to propose a consistent semi-phenomenological theory of photoinduced charge-carrier relaxation in 2D TMDs, which allows an analytical dependence of the quantum yield on the voltage applied to the field effect transistor gate to be obtained. We consider a standard experimental situation, when the 2D TMD monolayer and the metal gate are plates of a flat capacitor, and the capacitor charge is proportional to the gate voltage. Owing to very strong electron-hole interaction in TMD monolayers, quantum yield on the gate voltage and the carrier generation rate have been calculated for the cases of the prevailing recombination of excitons (radiative and Auger recombination). Analytical expressions are derived for the dependence of quantum yield on the gate voltage and photoinduced carriers generation rate at a fixed gate voltage. Quantitative agreement with experiment allows us to draw conclusions about the relevance of the proposed theoretical model for the description of carrier photogeneration and recombination in 2D TMD monolayers. The obtained results demonstrate the possibilities of 2D TMD quantum yield control by the gate voltage and indicate that 2D TMDs are promising candidates for modern optoelectronics devices.

DOI: 10.1103/PhysRevApplied.13.014040

I. INTRODUCTION

In recent years, there has been an active study of two-dimensional (2D) transition-metal dichalcogenides (TMDs), such as MoS_2, WSe_2, and $MoTe_2$ [1–3]. Many theoretical and experimental studies are devoted to the band structure and electronic properties of 2D TMDs [4–10], which demonstrate a possibility to tune the properties in a wide range owing to mechanical strain [4,5], and/or additional impurities [10]. In particular, the direct observation of the transition from an indirect to a direct band-gap state has been reported in monolayer $MoSe_2$ [6]. Possible applications of 2D TMDs have been studied in combination with bilayer graphene [11] (possibility to tune the electronic structure of MoS_2) and as 2D hybrid semiconductor-ferroelectric structure [12] (ultrafast, nonvolatile multilevel memory devices with nondestructive low-power readout).

2D TMDs, such as MoS_2 and WSe_2, unlike semimetallic graphene, have semiconductor properties, and unlike indirect-gap bulk TDMs, are direct-gap semiconductors, and therefore can be widely used in optoelectronics devices (see, e.g., Refs. [13–15]). The theory of photocarrier relaxation in 2D TMDs was developed by Kozawa et al. [16]. They assumed that the quantum yield (QY) in 2D TMDs is low owing to the separation by the internal field of the photoinduced electrons and holes to different points in the Brillouin zone (electrons come to the Λ point and holes come to the Γ point). The separation reduces the probability of the carriers' radiative recombination in the K point, where the top of the valence band and the bottom of the conduction band are located. However, when the carriers are excited by light quants of relatively low energy, only a

*anna.n.morozovska@gmail.com

small fraction of them are photoinduced in the part of the Brillouin zone, where a "band-nesting" effect is possible and, hence, the QY values may be higher.

Recent experiments [17] reveal the dominant role of dark exciton states in acid-treated MoS_2, and show that the excitons spend almost all of their lifetime at room temperature in trap states below the band edge. Goodman et al. [17] suggested that the exciton states are associated with native structural defects, which are not introduced by the acid treatment. The acid treatment strongly reduces nonradiative recombination through these states, extending the exciton lifetime and increasing the likelihood of eventual radiative recombination.

Recently, it has been shown experimentally [18] that the QY in monoatomic layers of MoS_2 and WSe_2 can reach values close to unity under electrostatic doping of these materials to the intrinsic semiconductor state. However, the theoretical description given in Ref. [18] being relevant *per se*, at the same time does not provide a clear understanding of why the QY is strongly dependent on the gate voltage and what happens with its changes. Therefore, the aim of our work is to construct a consistent semiphenomenological theory of the photoinduced carrier relaxation in 2D TMDs, which allow the analytical dependence of the QY value on the voltage applied to the field effect transistor (FET) gate to be obtained.

II. THEORETICAL MODEL

A. Problem statement

Here we consider a standard experimental situation. A 2D TMD monolayer and a metal gate are the plates of a flat capacitor, and the charge of each plate per unit area is equal to

$$Q = C_{\rm ox}(V_g - V_T), \tag{1}$$

where $C_{\rm ox}$ is the specific capacitance per unit area determined by the dielectric constant of the substrate and its thickness, and V_g is the gate voltage. The presence of V_T in Eq. (1) reflects the fact that doping defects are always present in 2D TMDs. For instance, 2D TMDs studied in Ref. [18] had *n*-type conductivity, and it was necessary to apply a negative gate voltage -20 V to transform them to the intrinsic semiconductor state. Considering further that the 2D TMD without gate doping is electronic (which corresponds to the standard experiments [15]), we write a simple expression for the "doping" voltage V_T:

$$V_T = \frac{eN_D}{C_{\rm ox}}, \tag{2}$$

where e is the elementary charge and N_D is the concentration of ionized donors. The geometry of the situation under consideration is shown in Fig. 1. Source and drain electrodes are implemented in order to obtain an optoelectronic

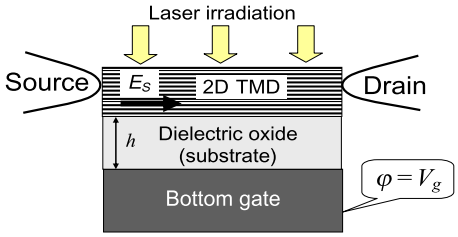

FIG. 1. Structure of the FET consisting of 2D TMD monolayer-dielectric oxide-bottom gate. The 2D TMD channel is stretched between the source and drain electrodes. Arrows indicate that a laser radiation illuminates the surface of the 2D TMD monolayer.

device instead of a mere flat capacitor. However, in the following we neglect a weak electric field between source and drain inside the channel in comparison with a strong field caused by a gate electrode.

The 2D MoS_2 and WSe_2 monolayers, in contrast to the corresponding indirect-gap bulk materials not suitable for optoelectronics, are direct-gap semiconductors with an optical gap $E_g \sim 1.8$ eV and with extrema of the conduction and valence bands in points K, K' of the hexagonal Brillouin zone [14,15], just as in graphene. The spectrum of the conduction band of these materials also contains a side extremum located in the direction from the points K, K' to the center Γ of the Brillouin zone. The presence of two subbands in the conduction band causes the possibility to realize the negative differential conductivity in the 2D WSe_2 and MoS_2. The effect is associated with the occupation of a higher valley with a higher effective mass by hot electrons (see the theory proposed in Ref. [19]).

Two important features of the 2D TMD band structure should be emphasized. The spin degeneration of the valence band at the points K, K' is removed by the spin-orbital interaction, but remains for the bottom of the conduction band [14,15]. The magnitude of the spin splitting of the valence band top in the 2D TMD is quite significant (about 160 meV for MoS_2 and 180 meV for $MoSe_2$), therefore we can assume that only the upper valence subband is occupied by holes at room temperature. The second feature is that the Coulomb interaction between electrons and holes increases significantly in the monoatomic TMD layers [14], and the optical gap becomes significantly smaller than the electronic gap, which appears in the expressions for electron and hole concentrations. For MoS_2, the exciton binding energy is at least 0.48 eV [14], and therefore the electronic gap is about 2.3 eV.

In the following, we consider the relatively low levels of photogeneration, when the equilibrium and nonequilibrium carrier concentrations are

$$n = n_o + \delta n, \quad p = p_o + \delta p, \tag{3a}$$

$$n_o \gg |\delta n| \quad p_o \gg |\delta p|. \tag{3b}$$

We assume that the equilibrium carriers are nondegenerated. The assumption corresponds to the experimental situation [18], when the Fermi level is located deep enough in the band gap. Considering the double valley degeneration in 2D TMDs (see, e.g., the review in Ref. [20] and references therein) the concentrations of nondegenerate equilibrium 2D electrons and holes are

$$n_o = \frac{2m_c}{\pi\hbar^2} e^{-[(E_c-E_F)/kT]} \equiv N_c e^{-[(E_c-E_F)/kT]},$$
$$p_o = \frac{m_v}{\pi\hbar^2} e^{-[(E_F-E_v)/kT]} \equiv N_v e^{-[(E_F-E_v)/kT]}. \quad (4)$$

Here $E_{c,v}$ are the energies of the conduction and the valence band edges at K and K' points, E_F is the Fermi level energy, $N_{c,v}$ are the effective densities of states in the conduction and valence bands, and $m_{c,v} = \sqrt{m_{c,v}^{||} m_{c,v}^{\perp}}$ are the averaged effective masses of carriers in the anisotropic conduction and valence bands, respectively. Note that the values N_c and N_v in Eq. (4) also differ by a factor of 2, which is caused by the above-mentioned removal of the spin degeneracy of the valence band top. A standard expression inherent to bulk semiconductors follows from Eq. (4):

$$n_o p_o = N_c N_v e^{-(E_g/kT)} \equiv n_i^2. \quad (5)$$

Here n_i is the carrier concentration in the intrinsic semiconductor, the Fermi level of which is located in the middle of the gap. It should be emphasized that Eq. (5) contains the electronic gap value, which is equal to the sum of the optical value and the binding energy of the exciton, $E_g = E_g^{\text{opt}} + E_{\text{ex}}$.

Next, we rewrite expression (1) as

$$n - p = C_{\text{ox}} \frac{V_g - V_T}{e}. \quad (6)$$

Using expressions (5) and (6) and considering the inequalities (3b), we obtain the quadratic equation, $np = n\{n - C_{\text{ox}}[(V_g - V_T)/e]\} = n_i^2$, the solution of which is

$$n = \frac{C_{\text{ox}}(V_g - V_T)}{2e} + \sqrt{\left[\frac{C_{\text{ox}}(V_g - V_T)}{2e}\right]^2 + n_i^2}, \quad (7a)$$

$$p = \frac{n_i^2}{n} \equiv -\frac{C_{\text{ox}}(V_g - V_T)}{2e} + \sqrt{\left[\frac{C_{\text{ox}}(V_g - V_T)}{2e}\right]^2 + n_i^2}. \quad (7b)$$

From expressions (7), $n = p \approx n_i$ for $V_g = V_T$, and $n \approx C_{\text{ox}} V_g/e \gg p$ for $V_g \gg V_T$ corresponding to a sharply unipolar conductivity. Solutions for p-type TMD can be obtained from Eqs. (7), where the sign before the first term should be changed.

B. Recombination channels

In what follows, we can consider separately two cases of recombination: the first when almost all photoinduced carriers are free, and the second, when almost all photoinduced carriers at first bind into electrically neutral excitons and subsequently recombine (this case corresponds to experimental situation studied in Ref. [17]). It is clear that the first case takes place at sufficiently high temperatures, $kT \gg E_{\text{ex}}$, and the second case corresponds to relatively low temperatures, $kT \ll E_{\text{ex}}$. Generally speaking, in the second case, one should consider the binding of photoinduced carriers into trions and bi-excitons as well, but because their binding energy is much smaller than the binding energy of excitons, we neglect these possibilities in the first-order approximation. In particular, for MoS_2, the binding energy of the trion is about 18 meV [14], which is slightly lower than the thermal energy at room temperature. Hence, without loss of generality, we assume that the concentration of trions and bi-excitons is much smaller than the concentration of excitons, and so they will not significantly affect other channels of recombination, at least for the situation, examined in Ref. [18], where the QY reaches almost unity values for the intrinsic case. It should also be noted that, owing to the large exciton binding energy in the 2D TMD monolayers, the second case takes place for the vast majority of practical situations. However, for the sake of generality, we also consider the first case in brief. A detailed discussion of the first case can be found in Suppl. Mat. [21].

In the following, we consider two major relaxation channels of free photocarriers, the radiative recombination, which rate is proportional to the product of the electrons and holes concentrations (the recombination energy is taken away by the light quantum), and the nonradiative Auger recombination, when the recombination energy transfers to the third carrier through Coulomb interaction, and the carrier goes into an excited state in the band structure and then relaxes, transferring energy to the lattice phonons or substrate (Fig. 2). In addition, we neglect other recombination mechanisms, such as Shockley-Reed recombination through defects, because of their lower intensity [16]. For low levels of quantum generation, the energy of which does not far exceed the gap width, the effect of the photoinduced electrons and holes "nestling" can also be neglected [16].

C. Analytical expressions for QY

By definition, the QY is equal to the ratio of the radiative recombination rate (number of recombination acts per unit time in a unit volume) to the total rate of radiative and nonradiative recombinations. For the case of free-carrier recombination, the QY, denoted as "Y", can be presented

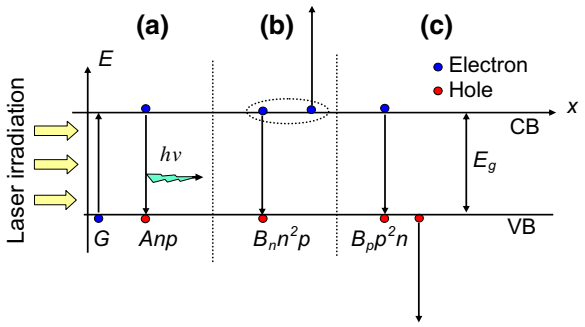

FIG. 2. Recombination processes in 2D TMDs: (a) radiative exciton recombination; (b),(c) nonradiative Auger recombination of an electron-hole pair with energy transfer to a third electron (b) or hole (c). A Coulomb interaction between the electrons inside the oval transmits the recombination energy. CB, conduction band; VB, valance band.

as

$$Y = \frac{T_R}{T_R + T_{\mathrm{NR}}} \approx \frac{Anp}{Anp + B_n n^2 p + B_p n p^2} \tag{8}$$

Here A is the coefficient of radiative recombination and $B_{n,p}$ are the coefficients of the nonradiative Auger recombination involving the second electron or hole, respectively. It may seem that nonradiative Auger recombination is *a priori* less efficient in sufficiently wide-gap semiconductors, such as 2D TMDs. The fact is that the simultaneous implementation of the energy and momentum conservation laws imposes the process threshold, and so it is possible only when the total kinetic energy of the three carriers involved in it is higher than a certain threshold energy, E_T, and therefore the Auger recombination coefficient B contains an exponential dependence $B \sim e^{-(E_T/kT)}$ [22]. Assuming parabolic bands with effective mass ratios $m_v \gg m_c$ it is easy to show that $E_T = (m_c/m_v)E_g$. Therefore, the threshold energy can be orders of magnitude higher than 0.026 eV, in a wide-gap semiconductor, and so the intensity of Auger-recombination is extremely low even at room temperature. However, the threshold E_T can be reduced significantly owing to the peculiarities of the band structure. Namely, if another parabolic valley with an effective mass m_c^{Δ} exists above the bottom E_c of the conduction band, and the energy gap $\Delta E \le E_g$ separates it from the bottom [see Fig. 3(b)], it is easy to show that the threshold energy is $E_T = (m_c^{\Delta}/m_v)(E_g - \Delta E)$, and it can be small enough if ΔE is close to E_g. The calculations [4,13–15] show that the 2D TMD band structure contains upper valleys for both the conduction and valence bands meeting the requirement, $E_g - \Delta E \ll E_g$, and therefore we can expect high coefficients $B_{n,p}$ in these materials. This means that Auger recombination can be intensive enough and significantly reduce the QY for high concentrations of carriers.

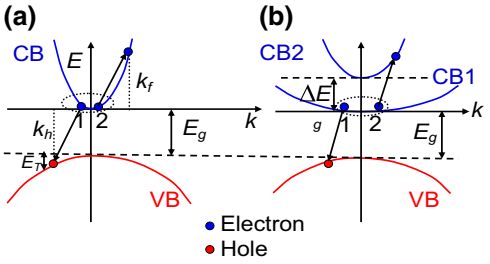

FIG. 3. Threshold for Auger recombination in the system with two (a) and three (b) bands. Coulomb interaction transmits the recombination energy of the order of the gap width between the electrons 1 and 2. The expressions $E_T \approx (\hbar^2 k_h^2/2m_v)$ and $|k_h| \approx (\sqrt{2m_c E_g}/\hbar)$ are true for (a), and the expressions $|k_h| \approx |k_f|$ and $|k_h| \approx [\sqrt{2m_c^{\Delta}(E_g - \Delta E)}/\hbar]$ are valid for (b) from the energy and momentum conservation laws.

We can rewrite expression (8) for QY as a function of electron concentration n:

$$Y[n] = \frac{1}{1 + (B_n/A)(n + \beta p)} \approx \frac{1}{1 + \alpha[n + \beta(n_i^2/n)]}, \tag{9}$$

where the parameters $\alpha = (B_n/A)$ and $\beta = (B_p/B_n)$ are introduced. The QY is a function of n, and n is dependent on the gate voltage. QY reaches an extremum (maximum in the considered case) for n values determined from the condition $(dY/dn) = 0$, which exactly corresponds to $1 - \beta(n_i^2/n^2) = 0$. The condition $n^2 = \beta n_i^2$ along with voltage-independent condition $\beta = 1$ means that in the point of maximum QY, the semiconductor should become intrinsic $(n = n_i = p)$ under the corresponding gate voltage. Knowing the electron and/or hole lifetimes for different recombination processes, it is possible to estimate the parameters α and β. The values of N_d and n_i are determined by the 2D TMD sintering technology and ambience temperature, and can vary over a wide range of values.

Note that according to Eqs. (6) and (7), the carrier concentrations n, p and their difference $(n - p)$ depend on the voltage difference $V_g - V_T$ only, so it makes sense to plot the concentration and QY as functions of $V_g - V_T$.

As we have seen previously, in fact, for all real monoatomic 2D TMD layers, the exciton binding energy is very high and the inequality $kT \ll E_{\mathrm{ex}}$ is valid. Therefore, almost all free carriers, which can find a pair, bound into excitons. The concentration of excitons n_{ex} will be approximately equal to the concentrations of minority carriers, that is, electrons in p-type material and holes in n-type material.

In this case, the physical picture of the recombination processes depicted in Fig. 2 undergoes changes. In each case, the free electrons and holes do not recombine, only the electrons and holes bound in the excitons recombine, and therefore the recombination rate is no longer

proportional to the product np, but to the concentration n_{ex}. The rate of nonradiative Auger recombination appears proportional also to the concentration of majority carriers (electrons or holes), which are not bound in excitons, and the energy of the gap width order is obtained through Coulomb interaction. As the exciton wave function contains a complete set of momenta, the Auger-recombination process involving an exciton has no energy threshold, which increases its probability [22].

The correct expression for QY takes into account that almost all minority carriers are bound into excitons in the low-temperature approximation, and there are virtually no minority carriers capable to take away recombination energy; there are only majority carriers that can do this. Therefore, the Auger-recombination process with the participation of a free electron can only occur in the n-type 2D TMD, and the process with the participation of a free hole can only exist in the p-type 2D TMD (their rates are denoted in the following as $T_{NR}^{(n,p)}$). This leads to the expressions

$$Y_{(n)} = \frac{T_R}{T_R + T_{NR}^{(n)}} \approx \frac{A^{ex} n_{ex}}{A^{ex} n_{ex} + B_n^{ex} n_{ex}(n - n_{ex})}, \quad (10a)$$

$$Y_{(p)} = \frac{T_R}{T_R + T_{NR}^{(p)}} \approx \frac{A^{ex} n_{ex}}{A^{ex} n_{ex} + B_p^{ex} n_{ex}(p - n_{ex})}. \quad (10b)$$

Here A^{ex} is the coefficient of radiative exciton recombination and $B_{n,p}^{ex}$ are the coefficients of the nonradiative Auger recombination of an exciton with the participation of the second electron or hole, respectively. Note that the dimensions of the coefficients A^{ex} and $B_{n,p}^{ex}$ in Eqs. (10a) and (10b) are different from the dimensions of the coefficients A and $B_{n,p}$ in Eq. (8). Considering that for n-type 2D TMD, the concentration of excitons is approximately equal to the concentration of minority holes, $n_{ex} \approx p$, and for p-type 2D TMD, n_{ex} is defined by the concentration of minority electrons, $n_{ex} \approx n$, we rewrite expressions (10a) and (10b) as

$$Y_{(n)} \approx \frac{1}{1 + (n - p)/N_n} \quad (11a)$$

$$Y_{(p)} \approx \frac{1}{1 + (p - n)/N_p} \quad (11b)$$

The "characteristic" concentrations $N_n = (A^{ex}/B_n^{ex})$ and $N_p = (A^{ex}/B_p^{ex})$ are introduced. Note that the values $N_{n,p}$ have the dimension of 2D concentration in SI units. To simplify the numerical analysis, the results of which are presented in the following, we assume that $N_n = N_p = N_{ex}$.

An important consequence of expressions (11) is that the QY does not depend on the concentration of excitons, but is sensitive to the concentration of free carriers only. Expressions (11) also show that the QY reaches a maximum (100%) at $n = p$, corresponding to the intrinsic semiconductor state. The QY values smaller than 100% observed in the experiment [18], even for the case of the intrinsic semiconductor, can be explained by the fact that there are always other nonradiative recombination channels (e.g., through impurity centers), which are not considered in our simplified method.

The maximum of QY for the intrinsic case $n = p$, predicted by Eqs. (11a) and (11b), has a clear physical explanation, because practically all the electrons and holes are bound into excitons, and there are no additional free electrons and holes, which can enable the nonradiative Auger process for this case. Note that for the case $n = p$, trions cannot be formed because of the strong inequality in their binding energies, $E_{ex} \ll E_{tr}$. Therefore, the only way for excitons decay is radiatively. That explains well the principal experimental result of Ref. [18].

III. RESULTS AND DISCUSSION

A. Controlling QY by gate voltage

Figures 4 and 5 show the voltage dependences of QY calculated from Eqs. (11). The interpolation function $Y_{(n)} \approx Y_{(n)}\text{UnitStep}[n - p] + Y_{(p)}\text{UnitStep}[p - n]$, where UnitStep$[x]$ is the Heaviside step function, is used to generate the plots. The interpolation is "tailoring" of Eqs. (11a) and (11b), that is continuous at $n = p$ for arbitrary concentrations N_n and N_p, including the considered case $N_n = N_p = N_{ex}$.

Note that according to Eqs. (6) and (7), the carrier concentrations and their difference $(n - p)$ depend only on the voltage difference $V_g - V_T$, so it makes sense to plot the dependence of n, p, and QY on $V_g - V_T$. However, to demonstrate the separation of QY maxima, we show the dependences $Y[V_g]$ calculated for different doping voltages V_T in Figs. 4(b)–4(d).

Figure 4(a) shows the dependences of n and p on $V_g - V_T$ calculated from Eq. (7) for the capacitance $C_{ox} = 20$ nF/m^2. Figures 4(b)–4(d) show the QY dependences calculated from Eqs. (11) on the gate voltage V_g for different values of the doping voltage V_T and effective concentration N_{ex}. As one can see from Fig. 4(b), for a relatively small N_{ex}, the QY reaches values close to 100% only in a very narrow vicinity of $V_g = V_T$. When N_{ex} increases, the QY becomes higher in a wider range of gate voltages [see Figs. 4(c) and 4(d)]. Physically, this is explained by the fact that the Auger-recombination rate is substantially lower than the radiative recombination rate in the limiting case of high N_{ex}, which significantly increases QY.

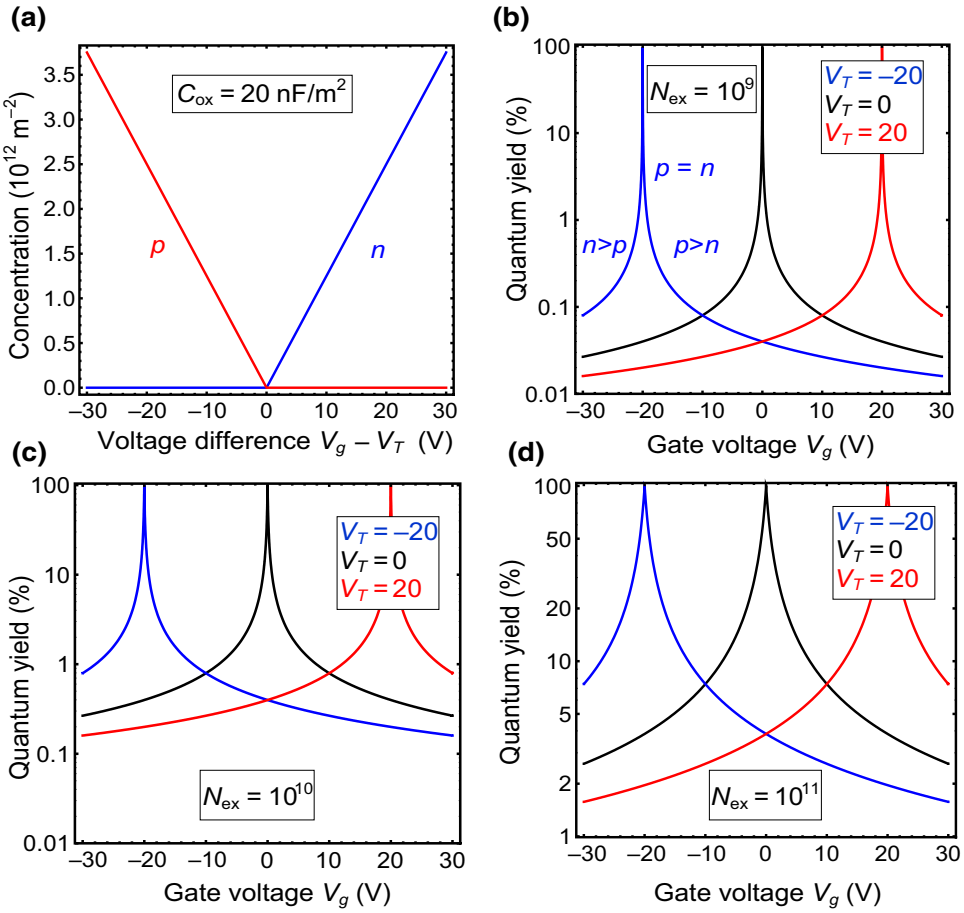

FIG. 4. (a) Dependence of carrier concentration calculated from Eq. (7) on voltage difference $V_g - V_T$ applied to 2D TMD. (b)–(d) Dependence of the QY on the gate voltage calculated from (14) for several values of the doping voltage $V_T = -20$, 0, and 20 V (blue, black, and red curves, respectively). Parameters $C_{ox} = 20$ nF/m^2, $n_i = 10^8$ m^{-2}, and $N_{ex} = 10^9$ m^{-2} (b), 10^{10} m^{-2} (c), and 10^{11} m^{-2} (d).

The dependence of 2D TMD QY on the voltage difference ($V_g - V_T$) and effective concentration N_{ex} calculated using Eqs. (11) for $C_{ox} = 2$ and $C_{ox} = 20$ nF/m^2 is shown in Figs. 5(a) and 5(b), respectively. It can be seen that the range of high QY increases linearly with increasing N_{ex}. The voltage range of high QY is symmetric with respect to $V_g - V_T$; and QY decreases significantly with C_{ox} increase. Results presented in Fig. 5 show a sharp character of the symmetric QY maximum at $V_g = V_T$.

B. Dependence of QY on generation rate

For comparison with experiment [18], we calculate the dependence of the QY (11) on the generation rate G at a fixed gate voltage, using approximate dependences of the concentrations of n and p on G.

To obtain the dependences $n(G)$ and $p(G)$, we take into account that the difference of negative and positive charges is described by expression (6) only for the case of small generation rates G, when the relation (3) holds. Then the

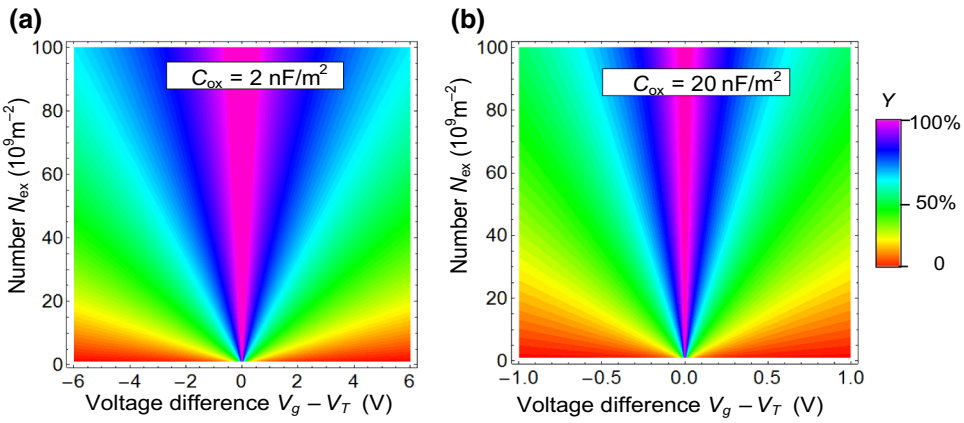

FIG. 5. Dependence of the 2D TMD QY on the voltage difference ($V_g - V_T$) and the effective concentration N_{ex} calculated from Eqs. (14) for the values $C_{ox} = 2$ nF/m^2 (a) and $C_{ox} = 20$ nF/m^2 (b). The other parameters are the same as in Fig. 6.

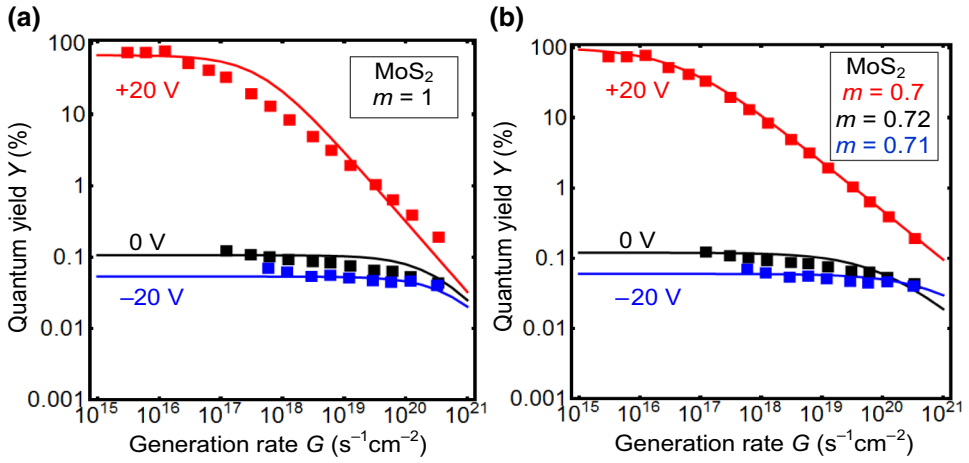

FIG. 6. The dependence of the QY on the generation rate G at several gate voltages. Symbols are experimental data [18] for the gate voltages +20 V (red), 0 (black), and −20 V (blue), red, black, and blue solid curves are fitted by Eqs. (13) for parameters (a) $V_T \approx 20$ V, $C_{ox} = 15$ nF/m^2, $N_{ex} = 1 \times 10^9$ m^{-2}, $m \approx 1$, $\tau_{eff} = 5 \times 10^{-9}$ s; (b) $V_T \approx 20$ V, $C_{ox} = 50$ nF/m^2, $N_{ex} = 3.75 \times 10^9$ m^{-2}, $m \approx 0.7$, $N_T(\tau_{eff}/N_0)^m = 7.84 \times 10^{-3}$ in SI units.

solutions (7) are valid, and the QY (11) does not depend on G, which corresponds qualitatively to the results of [17] for low intensities of generation.

For high generation rates Eq. (3a) is valid, and the inequalities (3b) do not hold, or even turn into inverse inequalities $n_o \le |\delta n|$ and $p_o \le |\delta p|$. If we consider the n-type 2D TMD with $n_o > p_o$ and the generation rate is high enough, then $n_o \sim \delta n$. We regard that there are many trapping levels for minority carriers, and the carriers are effectively captured by traps, and so $\delta n \gg \delta p$ (see, e.g., Ref. [22]). That is, there are free photoinduced electrons, but actually no free photoinduced holes, because they are immediately captured at the traps, much faster than all other processes occur. As a consequence, the electron concentration n in the denominator of Eq. (11a) is still described by Eq. (3a), but contains a nonequilibrium part that depends on G. The concentration of holes $p \approx p_o$, because the photoinduced carriers are immediately captured at the trapping levels, and cannot participate in the formation of excitons with free electrons. Of course, this is the simplest model of the recombination processes, because bound excitons and trions [18] can also be formed.

Thus, for the n-type doping the denominator in Eq. (11a) transforms as $n - p \to n_o + \delta n(G) - p_o$, and the dependence (11a) acquires the form

$$Y_{(n)}[G] \approx \frac{N_{ex}}{N_{ex} + \delta n(G) + C_{ox}[(V_g - V_T)/e]}. \quad (12a)$$

Equation (12a) is valid at $C_{ox}[(V_g - V_T)/e] \ge 0$. To compare it with experiment [18] it is necessary to obtain the dependence $\delta n(G)$. The simplest approximation is a linear function

$$\delta n(G) = \tau_{eff} G, \quad (12b)$$

which includes an effective lifetime τ_{eff} that, in general, can be very different from all other recombination times [22]. If there are many recombination channels and trapping levels, a power approximation can be used instead of (12b),

$$\delta n(G) \cong N_T \left(\frac{\tau_{eff} G}{N_0}\right)^m, \quad (12c)$$

where the factor m can be different from unity and is slightly dependent on V_g. The dimensionality of parameters N_T and N_0 is per square meter. Parameter m is simply a fitting parameter, the value of which can be less than unity for the case of a variety of rival recombination channels: at $m = 1$ for a single channel [see Eq. (12b)]. Actually, m value in the expression (12c) reflects the resulting contribution from different relaxation times into $\delta n(G)$. The situation is somewhat similar to the situation in different relaxors.

Similarly, p-type doping of 2D TMD in the presence of trapping levels for minority electron carriers leads to the substitution $p - n \to p_o + \delta p(G) - n_o$ in the denominator (12b), and the dependence (12a) acquires the form

$$Y_{(p)}[G] \approx \frac{N_{ex}}{N_{ex} + \delta p(G) - C_{ox}[(V_g - V_T)/e]}. \quad (12d)$$

Expression (12d) is valid at $C_{ox}[(V_g - V_T)/e] < 0$.

The dependence of QY on the generation rate G at a fixed gate voltage V_g is shown in Fig. 6. For the figure we use the interpolation function, $Y_{(n)} \approx Y_{(n)}\text{UnitStep}[n_o - p_o] + Y_{(p)}\text{UnitStep}[p_o - n_o]$, where UnitStep$[x]$ is a Heaviside step function, and consider two cases: $m = 1$ [Fig. 6(a)] and m is a fitting parameter [Fig. 6(b)].

The solid curves in both figures describe the experimental data [18] semiquantitatively and correspond to realistic values of the fitting parameters, $V_T \approx 20$ V, $C_{ox} = (15–50)$ nF/m^2, $N_{ex} = (1–4) \times 10^9$ m^{-2}, $m \approx 1$ or 0.7. To find the best agreement with experimental points [18], we vary the fitting parameters in a wide range, but reach the best fitting for the points at $V_g \approx 20$ V, because this case corresponds to the highest QY. The fitting of the experimental points at $V_g \approx 0$ and $V_g \approx -20$ V, corresponding to the much smaller QY, looks worse. The fitting

procedure involves a certain "weighting" of experimental points for each V_g, which are included into the least-squares functional and are adapted to minimize simultaneously the functional for three curves at $V_g = -20$, 0, and 20 V at the same fitting parameters.

Note that the satisfactory accuracy of the fitting for all three curves obtained at $m = 1$ and $m = 0.7$ corroborates the relevance of the proposed theoretical model to the physical processes of carrier generation and recombination in 2D TMD monolayers. A slight deviation of the parameter m from the value 0.7 in Fig. 6(b) means that the trapping of carriers is rather weakly dependent on the gate voltage. The effect is quite possible. For example, the density of the screening charges in a paraelectric or ferroelectric substrate is nonlinearly dependent on the applied voltage, not only on the screened polarization [23–25]. Moreover, to achieve a sufficiently large capacitance C_{ox} that increases the sensitivity of the FET (see Figs. 4 and 5), we may recommend the use of a ferroelectric or paraelectric perovskite oxides as a substrate. Thus, we state that proposed alternative simple model of the experiment [17], which does not include exotic recombination channels, such as trions and bi-excitons, allows the observed effects to be described on the same quantitative level. Moreover, this model gives clear physical understanding of maximum QY for the case of intrinsic TMD with $n = p$.

Finally, let us consider the question of the QY dependence on generation rate in the context of a more general model. The balance equation has the form

$$\frac{\partial n}{\partial t} = G + (\Delta^{ex} - A^{ex} n_{ex}) + (\Gamma_n^{ex} - B_n^{ex} n_{ex})(n - n_{ex}) + (\Gamma_p^{ex} - B_p^{ex} n_{ex})(p - n_{ex}). \tag{13}$$

Here the recombination and inverse ionization processes are gathered in brackets, Δ^{ex} and $\Gamma_{n,p}^{ex}$ are the coefficients that determine proper ionization rates [22]. Under the steady-state and thermal equilibrium conditions, each bracket on the right-hand side of Eq. (13) must be zero. This gives

$$\Delta^{ex} = A^{ex} n_{ex} \approx A^{ex}(p_o, n_o), \quad \Gamma_{n,p}^{ex} = B_{n,p}^{ex} n_{ex} \approx B_{n,p}^{ex}(p_o, n_o). \tag{14}$$

The concentration of intrinsic holes corresponds to the n-type 2D TMD and the intrinsic electrons to the p-type TMD in the brackets of Eq. (13). Keeping in mind the previous considerations regarding the expressions (12), we can rewrite Eq. (13) for the n- and p-type TMD in the case of not too high photoexcitation:

$$\frac{\partial n}{\partial t} = G + A^{ex}(p_o - p) + \Gamma_n^{ex}(n - p_o)(p_o - p) = G - [A^{ex} + \Gamma_n^{ex}(n - p_o)]\delta p \equiv G - \frac{\delta p}{\tau_{ex}^R} - \frac{\delta p}{\tau_{ex}^{NRn}}, \tag{15a}$$

$$\frac{\partial n}{\partial t} = G + A^{ex}(n_o - n) + \Gamma_n^{ex}(p - n_o)(n_o - n) = G - [A^{ex} + \Gamma_p^{ex}(p - n_o)]\delta n \equiv G - \frac{\delta n}{\tau_{ex}^R} - \frac{\delta n}{\tau_{ex}^{NRp}}. \tag{15b}$$

Here we assume that Eq. (3) is still valid, and the characteristic times of radiative and nonradiative exciton annihilation are introduced as

$$\tau_{ex}^R = \frac{1}{A^{ex}}, \quad \tau_{ex}^{NRn} = \frac{1}{\Gamma_n^{ex}(n - p_o)}, \quad \tau_{ex}^{NRp} = \frac{1}{\Gamma_p^{ex}(p - n_o)}. \tag{16}$$

Allowing for Eqs. (13) and (16) in the stationary case, we can rewrite the expression for the QY for the p-type and n-type TMD as

$$Y_{(n,p)} = \frac{\tau_{(n,p)}}{\tau_{ex}^R}, \quad \frac{1}{\tau_{(n,p)}} = \frac{1}{\tau_{ex}^R} + \frac{1}{\tau_{ex}^{NR(n,p)}}. \tag{17}$$

The total effective exciton annihilation times $\tau_{(n,p)}$ are introduced here. It is clear that when the exciton annihilation time is much smaller than the irradiation recombination time, the QY tends to unity. An important consequence of Eq. (17) is that the QY in the case of sufficiently low recombination rates does not depend on the generation rate G, but only on the concentrations of electrons and holes. However, as G increases and we go beyond the last of relations (3), because the concentrations in denominators (12) increase linearly with G, the QY decreases, which corresponds to the experimental dependences [18] (see Fig. 6).

IV. CONCLUSION

This work is an attempt to propose the self-consistent semiphenomenological theory of the photoionized carrier relaxation in 2D TMDs, which allows the analytical dependence of the QY on the voltage applied to the gate of the FET to be derived.

We consider the standard experimental situation when the 2D TMD monolayer and the FET gate are plates of a flat capacitor, and the charge of each of plate is proportional to the gate voltage. The dependences of the QY on

the gate voltage and intensity of carrier generation rate are calculated and analyzed.

The cases of dominant free electrons and holes recombination (radiative and nonradiative Auger recombination) and recombination of excitons (radiative and Auger recombination) are considered. In the first-order approximation, we neglect other less-intensive recombination channels, such as Shockley-Reed recombination, recombination of trions and bi-excitons, etc. Analytical expressions are derived for the concentrations of charge carriers and for the dependence of QY on the gate voltage, and the photocarriers generation rate at fixed gate voltage.

It appears that for real 2D TMD monolayers the second case dominates, because the binding energy of excitons is very high (0.5 eV or more [14]) owing to the strong electron-hole interaction in the monolayer, and therefore virtually all the minority carriers are bound into excitons at room temperature. Some of the majority carriers remain free, which allow Auger recombination by "taking away" the energy of the optical gap width order.

In both cases of free carriers and excitons recombination, the value of the QY reaches the maximum (order of unity) for the gate voltages corresponding to the intrinsic semiconductor state of 2D TMD monolayer (i.e., when the concentration of free electrons is equal to the concentration of free holes). In the second case, the reason for this is particularly physically transparent, because the free carriers capable of providing a nonradiative Auger-recombination process (and forming trions) are practically absent, and the recombination process occurs only through the radiative channel, except for Shockley-Reed recombination processes of lower intensity.

Quantitative agreement with experiment [18] (shown in Fig. 6) allows us to conclude about the relevance of the proposed theoretical model for the description of carrier photogeneration and recombination in 2D TMD monolayers. The obtained results demonstrate the possibilities of 2D TMD QY control by the gate voltage and indicate that 2D TMDs are promising candidates for modern optoelectronics devices.

ACKNOWLEDGMENTS

A.N.M. is grateful to Eugene A. Eliseev (NASU) for the assistance in processing and fitting of experimental results. The authors are very grateful to the referees for stimulating discussions and useful suggestions. The work of A.N.M. is supported by the National Academy of Sciences of Ukraine and has received funding from the European Union's Horizon 2020 research and innovation programme under the Marie Skłodowska-Curie Grant Agreement No. 778070.

M.V.S. formulated the concept, performed all analytical calculations and wrote the manuscript draft. A.N.M. and A.I.K. performed numerical calculations. A.N.M. compared with experiment, generated figures, and improved the text.

[1] S. Song, D. H. Keum, S. Cho, D. Perello, Y. Kim, and Y. H. Lee, Room temperature semiconductor–metal transition of $MoTe_2$ thin films engineered by strain, Nano Lett. **16**, 188 (2015).

[2] S. Kang, S. Jeon, S. Kim, D. Seol, H. Yang, J. Lee, and Y. Kim, Tunable out-of-plane piezoelectricity in thin-layered $MoTe_2$ by surface corrugation-mediated flexoelectricity, ACS Appl. Mater. Interfaces **10**, 27424 (2018).

[3] K.-A. N. Duerloo, Y. Li, and E. J. Reed, Structural phase transitions in two-dimensional Mo-and W-dichalcogenide monolayers, Nat. Commun. **5**, 4214 (2014).

[4] P. Johari and V. B. Shenoy, Tuning the electronic properties of semiconducting transition metal dichalcogenides by applying mechanical strains, ACS Nano **6**, 5449 (2012).

[5] S. Ahmad and S. Mukherjee, A comparative study of electronic properties of bulk MoS_2 and its monolayer using DFT technique: Application of mechanical strain on MoS_2 monolayer, Graphene **3**, 52 (2014).

[6] Y. Zhang, T.-R. Chang, B. Zhou, Y.-T. Cui, H. Yan, Z. Liu, and F. Schmitt, Direct observation of the transition from indirect to direct bandgap in atomically thin epitaxial $MoSe_2$, Nat. Nanotechnol. **9**, 111 (2014).

[7] N. Onofrio, D. Guzman, and A. Strachan, Novel doping alternatives for single-layer transition metal dichalcogenides, J. Appl. Phys. **122**, 185102 (2017).

[8] W. Wang, C. Yang, L. Bai, M. Li, and W. Li, First-principles study on the structural and electronic properties of monolayer MoS_2 with S-vacancy under uniaxial tensile strain, Nanomaterials **8**, 74 (2018).

[9] M. Drüppel, T. Deilmann, J. Noky, P. Marauhn, P. Krüger, and M. Rohlfing, Electronic excitations in transition metal dichalcogenide monolayers from an LDA+ GdW approach, Phys. Rev. B **98**, 155433 (2018).

[10] J. Suh, T. L. Tan, W. Zhao, J. Park, D.-Y. Lin, T.-E. Park, and J. Kim, Reconfiguring crystal and electronic structures of MoS_2 by substitutional doping, Nat. Commun. **9**, 199 (2018).

[11] Z. B. Aziza, H. Henck, D. Di Felice, D. Pierucci, J. Chaste, C. H. Naylor, A. Balan, Y. J. Dappe, A. C. Johnson, and A. Ouerghi, Bandgap inhomogeneity of MoS_2 monolayer on epitaxial graphene bilayer in van der waals pn junction, Carbon **110**, 396 (2016).

[12] T. Li, P. Sharma, A. Lipatov, H. Lee, J.-W. Lee, M. Y. Zhuravlev, T. R. Paudel, Y. A. Genenko, C. B. Eom, E. Y. Tsymbal, and A. Sinitskii, Polarization-mediated modulation of electronic and transport properties of hybrid $MoS_2 - BaTiO_3 - SrRuO_3$ tunnel junctions, Nano Lett. **17**, 922 (2017).

[13] P. Miro, M. Audiffred, and T. Heine, An atlas of two dimentional materials, Chem. Soc. Rev. **43**, 6537 (2014).

[14] X. Li, L. Tao, Z. Chen, H. Fang, X. Li, X. Wan, J.-B. Xu, and H. Zhu, Graphene and related two-dimentional materials: Structure-property relationship for electronics and optoelectronics, Appl. Phys. Rev. **4**, 021306 (2017).

[15] O. V. Yazyev and A. Kis, Mos_2 and semiconductors in the flatland, Mater. Today **18**, 20 (2015).

[16] D. Kozawa, R. Kumar, A. Carvalho, A. K. Kumar, W. Zhao, S. Wang, M. Toh, Ricardo M. Ribeiro, A. H. Castro Neto, K. Matsuda, and G. Eda, Photocarrier relaxation in two-dimensional semiconductors, Nat. Commun. **5**, 4543 (2014).

[17] A. J. Goodman, A. P. Willard, and W. A. Tisdale, Exciton trapping is responsible for the long apparent lifetime in acid-treated MoS_2, Phys. Rev. B **96**, 121404(R) (2017).

[18] D.-H. Lien, S. Z. Uddin, M. Yeh, M. Amani, H. Kim, J. W. Ager, E. Yablonovitch, and A. Javey, Electrical suppression of all nonradiative recombination pathways in monolayer semiconductors, Science **364**, 468 (2019).

[19] V. G. Lytovchenko, A. I. Kurchak, and M. V. Strikha, Theoretical model for negative differential conductance in 2D semiconductor monolayers, Ukr. J. Phys. **63**, 527 (2018).

[20] Yu. A. Kruglyak and M. V. Strikha, Generalized Landauer-Datta-Lundstrom model in application to transport phenomena in graphene, Ukr. J. Phys. Rev. **10**, 3 (2015).

[21] See Supplemental Material at http://link.aps.org/supplemental/10.1103/PhysRevApplied.13.014040 for calculations of quantum yield in monolayer transition-metal dichalcogenide conditioned by the recombination by free electrons and discussion of the mechanism.

[22] V. N. Abakumov, V. I. Perel, and I. N. Yassievich, Nonradiative Recombination in Semiconductors, North Holland (1991).

[23] S. V. Kalinin, Y. Kim, D. Fong, and A. Morozovska, Surface screening mechanisms in ferroelectric thin films and its effect on polarization dynamics and domain structures, Rep. Prog. Phys. **81**, 036502 (2018).

[24] A. I. Kurchak, A. N. Morozovska, E. A. Eliseev, S. V. Kalinin, and M. V. Strikha, Nontrivial temperature behavior of the carrier concentration in the nanostructure graphene channel on ferroelectric substrate with domain walls, Acta Mater. **155**, 302 (2018).

[25] A. N. Morozovska, E. A. Eliseev, I. S. Vorotiahin, M. V. Silibin, S. V. Kalinin, and N. V. Morozovsky, Control of polarization hysteresis temperature behavior by surface screening in thin ferroelectric films, Acta Mater. **160**, 57 (2018).